Scientific paper

Mixing Times in a Stirred Vessel with a Modified Turbine

Andrej Bombač,[1,*] Dečan Beader[2] and Iztok Žun[1]

[1] *University of Ljubljana, Faculty of Mechanical Engineering, Aškerčeva 6, 1000 Ljubljana SI,*

[2] *AVL-AST d. o. o., Trg Leona Štuklja 5, 2000 Maribor SI*

* *Corresponding author: E-mail: andrej.bombac@fs.uni-lj.si*

Received: 08-05-2012

Abstract

We present a mixing-time analysis for a double-disk turbine (DDT, SI Pat.No. 22243) and the well-known Rushton turbine (RuT) based on liquid stirring in a baffled vessel. The mixing time was measured locally based on the pulse/response technique. A small quantity of hot water, poured into the liquid bulk, just above the measurement location, was used as the pulse, while the change in the liquid temperature represented the system response. The results were obtained in two ways: (i) from measurements on the set-up and (ii) based on a CFD analysis. The pouring of the hot water was numerically simulated through the initialization of the scalar field. The duration of the temperature-pulse initialization around the measuring location corresponded to the pouring time in the experiment. All the energy introduced was freely swept away by the flow. The CFD-analyzed mixing times were consistently higher than the measured ones across the whole testing range, from 150 to 460 min^{-1}. When comparing our mixing-time results with those from the literature based on a dimensionless mixing time we found them to be in good agreement.

Keywords: Disk/double-disk turbine, mixing power, mixing time, temperature response, computational fluid dynamics

1. Introduction

Mixing time is generally used as a unique parameter that characterizes the mixing efficiency of different types of impellers: the impeller that achieves the shortest mixing time for the same power dissipation is considered to be the most efficient.

In most cases the power dissipation primarily depends on the transport and rheological properties of the media, the different geometrical ratios between the impeller and the vessel, and the type of impeller.[3,4,5,8,9,10,14] A higher impeller speed increases the power dissipation as well as the pumping capacity of the impeller and, consequently, results in a shorter mixing time. To improve the mixing performance, especially in gassed systems, many variations of the impeller shape have been developed, such as, e.g., the low-power hydrofoil impeller[8] or the novel hollow-blade impeller,[9] as well as a variety of modifications to the impeller blade[6,9–13] in order to avoid flooding.[2,10,36] However, it is not just the impeller, various combinations of types and numbers of impellers,[25] tank-bottom shapes,[14] sizes and numbers of baffles,[15,16] and even a horizontally placed stirred vessel[17] have been the subject of intensive research.

To determine the mixing time many specially devised experimental methods can be found in the literature, e.g., temperature response,[10,34] discoloration,[1,5,37] conductivity,[5,6,14,16,17,27,37–39] or pH change,[7,10] and a laser-induced fluorescence technique,[35,40] to mention just a few of them. They are based on the measurement of different physical properties, so a straightforward comparison of the results should be treated carefully. In addition, there are also various criteria in use to determine the mixing time, depending on the desired degree (%) of homogeneity. Values such as 30%[7], 90%[1,7,18], 95%[4,6,9,14,18–20] or 99%[5,14,31,38] are common in the literature. Fassano and Penney,[31] based on the idealized mixing decay model, developed a correlation to calculate the time required to reach a certain degree of homogeneity of the mixture in an agitated vessel. This correlation was found to be very appropriate for recalculating mixing times based on a different degree of homogeneity compared to the common one.

The variety of mixing-time measuring locations found in literature[7,14,20,23,34] also prevents any direct inter-

comparison of the results. In accordance with the Fluid Mixing Process consortium,[30] some experiments on the mixing time, following the FMP's recommendations, can be found in the literature.[7,14] In this way Haucine et al.[14] measured the mixing times below the surface, just below the turbine and near the vessel wall. The smallest variation in the local mixing time was found to be right below the surface, which was + 3.7% compared to the average of all three locations. In order to estimate the global mixing time more precisely, Diestelhoff et al.[35] measured the mixing times locally at 32 different locations across the tank. They reported that the measured local mixing times vary by as much as 39% between different points in the tank.

Recently, many computational fluid dynamics (CFD) techniques were employed to study the hydrodynamics in a stirred tank. In most of these CFD simulations the mixing time was determined by solving the Reynolds-averaged Navier-Stokes (RANS) equations with the standard k–ε turbulence model. These simulations showed under-predicted power numbers[18,20,24] and over-predicted mixing times.[7,18] Using the large-eddy-simulation (LES) approach researchers[23,40] showed a better prediction of the mixing times. A LES requires an enormous amount of computational power and it is not possible for very-large-scale industrial contactors at a high Reynolds number. In most cases it is necessary to understand the gross flow patterns.[26] However, this approach is very CPU-time consuming (computational cost) and is the major constraint in the modeling of mixing systems. For this reason, RANS-based models are preferred by many researchers for determining the power consumption and the mixing time.[7,18,41]

This paper presents a mixing-time analysis based on stirring in a pilot-sized vessel with a standard Rushton turbine and a modified, patent-pending disk turbine, which was developed in the Laboratory for Fluid Dynamics and Thermodynamics at the Faculty of Mechanical Engineering in Ljubljana. The standard Rushton turbine served for a comparison of the results from the two impellers and with the literature data. The mixing time was determined based on the pulse-response technique, where a small quantity of hot water was poured onto the liquid surface just above the measuring location (as a pulse), while the change of the liquid's temperature served as a system response. The results were obtained in two ways: (a) from measurements on the experimental set-up, and (b) from a CFD analysis, where the fluctuation of the temperature at the same location as in the experimental set-up was captured. The measuring position below the surface was chosen according to the results of Haucine et al.[14] as the most appropriate and handy location for conducting the experiment. The fair agreement between the experimental and the CFD results confirms the applicability of the simple and 'cheap' hot-water-based, pulse/response method. In general, based on both the experimental and the CFD results the local mixing time decreases with the amount of power being drawn.

2. Experimental

A cylindrical, flat-bottomed vessel was made of Perspex with a 450 mm ID, a liquid height equal to the

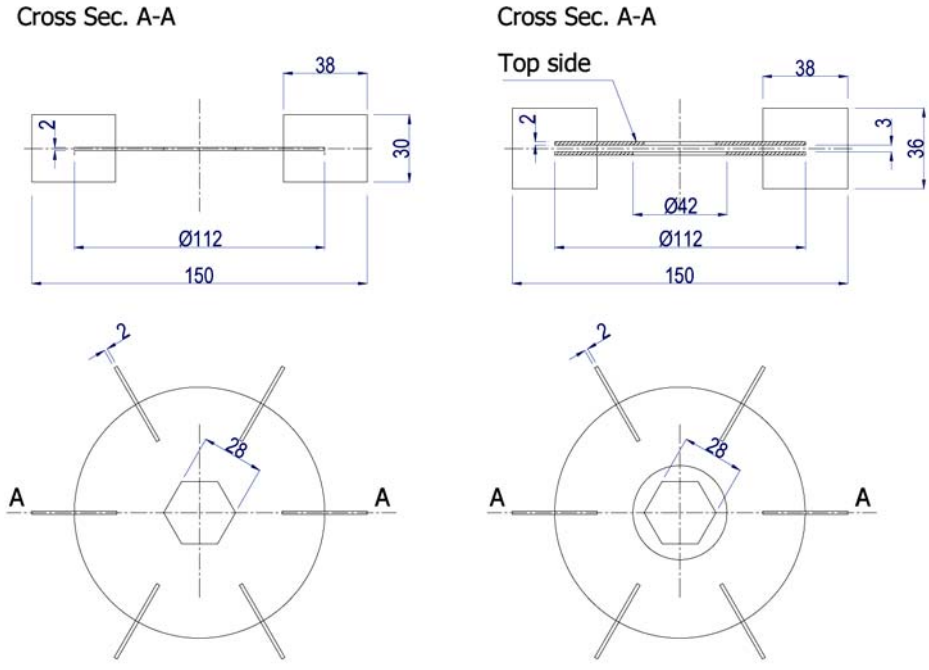

Figure 1. RuT impeller (left) and DDT impeller (right)

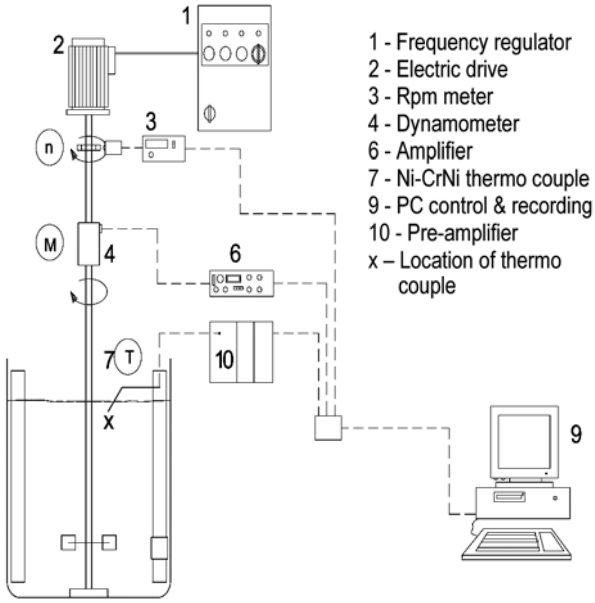

Figure 2. Experimental set-up

tank diameter (i.e., $H = T$), and an impeller-to-tank diameter ratio of 1/3. Four baffles were mounted perpendicularly to the vessel wall. The modified DDT impeller was composed of double, parallel, equal-sized disks of 112.5 mm diameter and six, equally spaced blades having the same width. The disks produce a layer of out-flowing water, which, for example, makes it possible to have a higher capability for gas dispersing. In addition, a standard Rushton turbine of 150 mm diameter and of same disk diameter (as for the DDT) was used for a comparison of the results. All the details of the used impellers are given in Figure 1.

The impeller was placed concentrically in the vessel on the impeller shaft at $H/3$. Deionized water of mass 70.35 kg at room temperature was used as the working fluid in all the experiments. The impeller speed was measured by an IR-pulse transmitter with an absolute error of ± 1 min^{-1}. An HBM transducer enabled torque measurements with an uncertainty of ± 0.02 Nm, as detailed in earlier studies.[29,36] The mixing time was measured based on the pulse-response technique, which is described elsewhere.[7,14,21] In our particular case one dm^3 of hot water at a temperature between 92 °C and 96 °C was added into the mixing liquid at a pouring time of ~1s, just above the location of the thermocouple tip, shown in Figure 2 as the mark x;{*r,z*: 65,420 mm} in the plane between baffles. This location was chosen based on literature data[14] as the most appropriate one. A non-insulated electrical thermocouple (Ni-CrNi, type K) with a 0.2 mm diameter tip was used to provide a very quick response. Based on three repeated measurements the temperature response of the thermocouple was found to be between 440 and 550 °C/s. Such a response is assumed to be fast enough to measure the mixing time in the analyzed stirring process. On the other hand, such a non-insulated thermocouple "receives" noise, which was effectively filtered out.

The temperature response of the NiCr-Ni thermocouple represented an arbitrary property of the 12-bit AD conversion, including the noise of higher frequencies (>5 kHz). A simple filtering process, based on a gradient method that eliminated all the responses faster than the thermocouple response, enabled further processing of the signal in order to derive the mixing time, as shown in Figure 3. The scanning frequency was set at 1000 Hz. In subsequent experiments the averaging from each of 100 samples was used to obtain the final rate of 10 samples/s.

The measuring time for all the experiments never exceeded 35 seconds. The temperature rise due to the mixing process itself was detected through a longer observation time (few hours), otherwise in our experiments it was negligible due to the short measuring time.

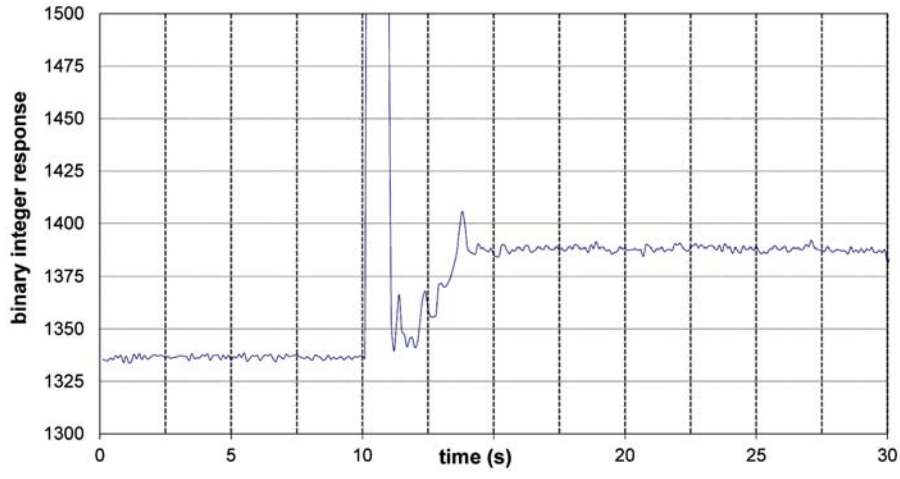

Figure 3. Temperature response

2. 1. Temperature Response as a Mixing-Time Criterion

In accordance with the first law of thermodynamics, the energy conservation for the control volume (i.e., the mixing tank) for the steady-state regime can be written as:

$$Q_{12} = \Delta U_{12} + W_m \tag{1}$$

where we denote the following: Q_{12} – heat exchanged with the surroundings, ΔU_{12} – change of the internal energy and W_m – work of mixing, i.e., the energy dissipated within the liquid. The exchanged heat can be neglected due the fact that the water temperature at the beginning is almost the same as the surrounding temperature, while after pouring the water the temperature is negligibly higher. The work of mixing (where the transport properties do not change with time within the control volume) can be assumed as:

$$W_m = Po \cdot \rho \cdot n^3 \cdot D^5 \cdot t_m \tag{2}$$

where we denote the following: Po – dimensionless power number ($P/\rho\, n^3 D^5$), P – mixing power, n – impeller speed, D – impeller diameter, ρ – liquid density and t_m – mixing time. The change of the internal energy is determined by the change of state before/after the adding of the „pulse“ water into the system:

$$\Delta U_{12} = c_w \cdot m_1 \cdot (T_F - T_1) + c_w \cdot m_2 \cdot (T_F - T_2) + C_a \cdot (T_F - T_a) \tag{3}$$

where we denote the following: m_1 – mass and T_1 – initial average temperature of the water in the vessel, m_2 – mass and T_2 – temperature of the added water, m_a – mass and T_a – temperature of the mixing device, T_F – final average temperature of the mixture, c_w – the specific heat of water, $c_a = \Sigma m_{ai} \cdot c_{ai}$ – the heat capacity of the mixing device, including all the parts, i.e., shaft, impeller, vessel, sparger, baffles, etc. In accordance with the small mass as well as the small specific heat of the elements involved, the heat capacity represents approximately 10% of the water's heat capacity. Finally, based on eqs. 1–3, the final temperature can be written as:

$$T_F = \frac{W_m + c_w (m_1 \cdot T_1 + m_2 \cdot T_2) + C_a \cdot T_a}{c_w (m_1 + m_2) + C_a} \tag{4}$$

which served as a control parameter for the mixing-time calculations. Based on a literature survey[6,14,31] a mixing-time criterion, obtained from the measured arbitrary properties, was applied by demanding a 95% degree of homogeneity. In this way the mixing time was defined as the time required for the temperature fluctuations to become smaller than 5% of the total temperature change using the given procedure:

The time step $t_{beg} = t_i$ was determined by the condition;

$$T_i \geq \mathrm{Avg}(T_{i-10};\, T_i) \cdot 1{,}05;\; i = 1, \ldots N\,,$$

where denotes: T_i – arbitrary temperature and t_i – time at i – step of the sample.
End time step $t_{end} = t_i$ was defined with the following condition:

$$T_i \geq \mathrm{Avg}(T_i;\, T_{i+10}) - 0{,}05 \cdot \Delta T \wedge T_i \leq (\mathrm{Avg}(T_i;\, T_{i+10}) + 0{,}05 \cdot \Delta T,\; i = 1, \ldots N\,, \tag{5}$$

where temperature difference denotes

$$\Delta T = T_{beg} - T_{end}.$$

T_F served as a control in the above procedure as a time stamp in the signal where the calculations were expected to stop.

The relative repeatability error of the mixing times based on three measurements in the same hydrodynamic regime was lower than 10%.

In the CFD simulations we also assumed that the introduced heat of the pulse-water is relatively small and the mixing process is fast enough to determine the mixing time in the transient mode. In control calculations in which a constant temperature and a constant (zero) heat flux were prescribed and all fluid equations solved, the difference was less than 5%. In the case where the velocity field was "frozen", the difference was almost negligible, as was expected. In the "frozen" flow-field simulations either constant temperature boundary conditions or zero heat flux boundary conditions could be adopted with practically no difference in the resulting mixing time regarding the used constant-temperature boundary condition.

2. 2. CFD Calculation of the Mixing Time

Using CFD calculations the following restrictions were applied: (i) the change of the water volume and rise of the water surface level (caused by pouring 1 dm^3 of hot water at 95 °C into the tank, which increased the mass of the system by approximately 1.45%) was neglected, (ii) the deformation of the surface level caused by the centrifugal force was also neglected, (iii) the water surface remained smooth.

On the basis of these assumptions the mixing process was assumed to be of a single-phase type. For such a system, the momentum, continuity and energy equations (governing set of equations) can be written in differential form for the liquid phase only as:

$$\frac{\partial \hat{\rho}}{\partial t} + \frac{\partial \hat{\rho} \hat{V}_i}{\partial x_j} = 0 \tag{6}$$

$$\hat{\rho}\frac{\partial \hat{V}_i}{\partial t}+\hat{\rho}\hat{V}_j\frac{\partial \hat{V}_i}{\partial x_j}=\hat{\rho}g_i-\frac{\partial \hat{p}}{\partial x_i}+\frac{\partial}{\partial x_j}\left[\mu\left(\frac{\partial \hat{V}_i}{\partial x_j}+\frac{\partial \hat{V}_j}{\partial x_i}-\frac{2}{3}\frac{\partial \hat{V}_k}{\partial x_k}\delta_{ij}\right)\right]-\hat{\rho}(2\hat{V}_k+\omega_l x_m \varepsilon_{lmk})\omega_j\varepsilon_{jkl} \quad (7)$$

$$\hat{\rho}\left(\frac{\partial \hat{\Omega}}{\partial t}+\hat{V}_j\frac{\partial \hat{\Omega}}{\partial x_j}\right)=\hat{\rho}\dot{q}_g+\frac{\partial \hat{p}}{\partial t}+\frac{\partial}{\partial x_i}(\hat{\tau}_{ij}\hat{V}_j)+\frac{\partial}{\partial x_i}(\lambda\frac{\partial \hat{T}}{\partial x_j}) \quad (8)$$

where we denote the following:

$$\hat{V}_i=\hat{U}_i-\omega_j x_k \varepsilon_{jkl},\ \hat{W}_i=\omega_j x_k \varepsilon_{jkl},$$

$$\hat{\Omega}=C_p\hat{T}+\frac{1}{2}(\hat{V}_i\hat{V}_i-\hat{W}_i\hat{W}_i)$$

and: V_i – relative velocity, ρ – density, g_i – gravitational vector, p – pressure, ω_i – vorticity, μ – viscosity, x_i – positional vector, U_i – velocity vector, ε_{ijk} – permutation symbol and λ – heat conductivity.

The equations (6–8) were solved numerically. The Reynolds averaging procedure (in which the flow field is approximated as the sum of its mean value and the instantaneous fluctuations) was adopted. As a result, two additional variables appeared, i.e., the turbulent stress tensor and the turbulent heat flux. These two quantities were modeled; otherwise additional transport equations had to be solved. From among the variety of available models, the standard k–ε turbulence model for high Reynolds numbers was adopted ($5.6 \cdot 10^4 < Re < 1.71 \cdot 10^5$). This approach contributed two additional equations to the system of equations (6-8), one for the turbulent kinetic energy (k) and another for its dissipation (ε), equations (9,10):

$$\rho\frac{\partial k}{\partial t}+\rho U_j\frac{\partial k}{\partial x_j}=P+G-\varepsilon+\frac{\partial}{\partial x_j}\left(\mu+\frac{\mu_t}{\sigma_k}\frac{\partial k}{\partial x_j}\right) \quad (9)$$

$$\rho\frac{D\varepsilon}{Dt}=\left(C_{\varepsilon 1}P+C_{\varepsilon 3}G+C_{\varepsilon 4}k\frac{\partial U_k}{\partial x_k}-C_{\varepsilon 2}\varepsilon\right)\frac{\varepsilon}{k}+\frac{\partial}{\partial x_j}\left(\frac{\mu_t}{\sigma_\varepsilon}\frac{\partial \varepsilon}{\partial x_j}\right) \quad (10)$$

where P is defined as:

$$P=-2\mu_t S:S-\frac{2}{3}\left[\mu_t(trS)+k\right](trS),$$

$$S=\sqrt{S_{ij}S_{ij}},\ G=-\frac{\mu_t}{\rho\sigma_\rho}\nabla\rho \text{ and } \mu_t=C_\mu\rho\frac{k^2}{\varepsilon}$$

Here, μ_t represents the turbulent viscosity and σ_k the turbulent Prandtl number, while $C_{\varepsilon i}$ is a model constant. In order to solve the above system of partial differential equations, a commercial CFD package was used. The necessary modifications due to the specific initialization process were implemented via user coding.

The CFD calculations were first validated against mixing-power measurements. The power number Po was calculated as $Po = P/\rho n^3 D^5$, where the impeller power is given as $P = 2\pi n\tau$ and τ is the total torque exerted on both the impeller shaft and the turbine. The torque was obtained by integration as $\tau = \int r \times F$, where **r** represents the distance vector between the observed surface element (face) and the axis of rotation. The calculations stopped when steady-state conditions were achieved.

Computational meshes: The computational meshes consisted of 489,800 and 602,550 cells for the Rush-

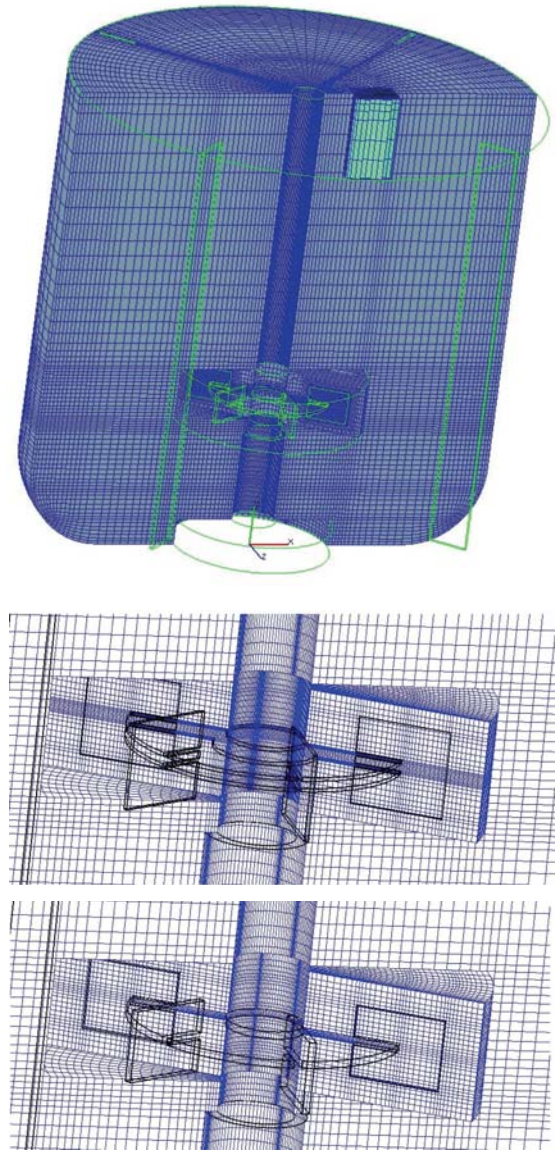

Figure 4. Computational mesh with detailed impeller region: DDT (top) and RuT (bottem)

ton turbine (RuT) and the Double-disk turbine (DDT), respectively. The near-wall mesh was of such a density that consistent use of a standard wall function was justified (averaged y^+ ranged from 31 to 139 on the vessel wall, from 17.2 to 79 on the stirrer, and from 23.2 to 104.4 on the shaft). A combination of block-structured meshes, see Figure 4, was used. All the meshes were generated within the preprocessor of the CFD package.[22]

Initial and boundary conditions: The vessel was initially filled with water at room temperature (T_1 = 293,15K). Room temperature was also prescribed as a boundary condition for the vessel walls and the impeller shaft walls. Also, a non-slip boundary condition was prescribed at the vessel walls. A predefined circular velocity corresponding to the rotational frequency was imposed on the impeller shaft. The water surface was considered to be smooth and its level stationary. Therefore, the normal velocity and normal fluxes of all the variables across the surface were set to zero.

Convergence criterion: In the case of the DDT the convergence criterion was satisfied if the reduction of the residuals dropped below $1 \cdot 10^{-3}$, except in the case of a scalar, where $1 \cdot 10^{-7}$ was set as a limit in order to fully test its convergence rate. Similar settings were used for the RuT, smaller than $1 \cdot 10^{-4}$, and smaller than $1 \cdot 10^{-5}$ in the case of a scalar. In order to determine the mixing time, the temperature fluctuation was defined according to Eq.5. If the amplitude of its oscillation dropped below 5% of its final mean value at the measuring location, the mixing time was considered to have been achieved.

Impeller-baffles interaction: Since the baffles were located far enough from the impeller, their influence on the flow field near the impeller was assumed to be minimal, so the "Multiple reference frame" technique was applied. In this approach, motivated by the large reduction in the CPU power needed, the impeller zone was treated separately in a rotating coordinate system (rotational framework). Here, the influence of the rotation is captured via additional source terms due to the centrifugal force. Within the impeller zone a system of equations (6-10) was solved as a whole. In contrast, outside the impeller zone in a stationary framework (which was the major part of the computational domain) a reduced system of equations was solved. Here, the terms due to rotation were absent and the relative velocity vector V_i was formally replaced with the velocity vector U_i. The converged solution was obtained upon iteration.

Simulation strategy: In a simulation of passive scalar transport, there is only a one-way interaction with the flow field, i.e., the instantaneous velocity affects the scalar evolution, while the passive scalar does not influence the flow characteristics. In this way the scalar field is mathematically decoupled from the dynamical equations that govern the flow field and the solution of the flow field is thus a prerequisite to the solution of the scalar field. Therefore, a well-validated and fully developed turbulent flow field was used to solve the transient passive scalar (temperature) transport equation.[23] Initially, before adding the hot water was attempted and in order to further reduce the required CPU time the system of equations (6-10) was solved (MRF, steady-state calculation). As soon as the steady-state conditions were achieved the calculation of the velocity field was stopped and "frozen". In this manner, the CPU time was reduced considerably (by up to 6-7 times). Afterwards, the simulations were continued in transient mode. The temperature (normalized) was kept initiated with a value of 1 in the control volume around the measuring point, as long as the appropriate mixture fraction of hot water reached the value corresponding to the final volume of the added hot water. This state was achieved within the first second (approximately) of the simulation (at n = 266 min^{-1}). The initialization period corresponded to the real time in which the hot water was poured into the vessel. All the simulations ran for 30 s of real time. The mean temperature achieved at the end of the simulation is assumed to be the final temperature T_F. The mixing time was then determined on the basis of the temperature fluctuations at the same location as with the experiment.

3. Results and Discussion

The CFD simulation results were compared with the experimental ones conducted in this study and with those reported in the literature. In the experimental measurements a set of power-consumption and mixing-time data was collected for impeller speeds of n = 100, 150, 200, 240, 266, 300, 350, 376, 400, 440, 460, and 500 min^{-1}. Due to time and costs restrictions associated with the CFD analyses only six impeller speeds were selected, i.e., 150, 200, 266, 376, 400, 460 min^{-1}. For the DDT impeller the developing of a flow field was converged after 1425 iterations with a four-core processor in 2193 sec. On the other hand, the calculation of the mixing time for 30 sec of transition ran to 159144 sec in spite of the proposed "frozen regime" method.

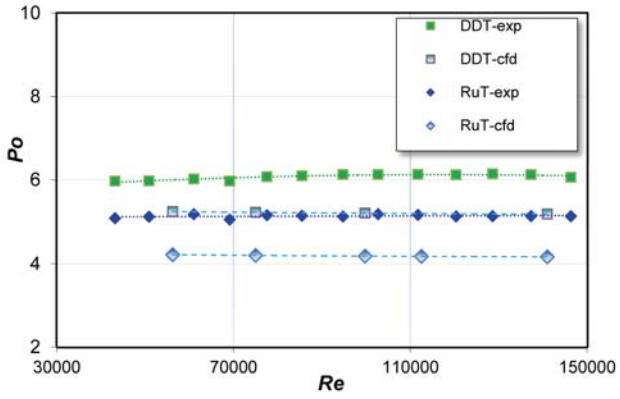

Figure 5. Experimental and CFD analyzed Power number of impellers

3. 1. Mixing Power

The mixing power of both impellers was measured directly at the impeller shaft for different impeller speeds. The corresponding dimensionless numbers are shown in Figure 5 (filled marks) in the graph of *Po* vs. *Re* number.

For both impellers the surface aeration appeared with increasing impeller speed at the corresponding *Re*≈135000. The averaged Power numbers in the single-phase mixing were found to be 6.04 for the DDT and 5.15 for the RuT impeller. According to the literature survey the *Po* number of the standard Rushton turbine varies considerably and is reported to be in between 4.8 to 6.3.[3,21,12] The measurements showed that the DDT impeller achieved an approximately 17% higher *Po* value than the RuT one. The reason is the higher blades, which caused a more intensive radial outflow, and in the additional outflow from the 'channel' between the disks.

This can be clearly seen from the CFD-analyzed plots in Figure 6, which show the velocity vectors in the middle *r-z* plane between two baffles. The larger area of higher velocities in the outflow in the case of the DDT compared to the RuT is also reflected in higher *Po* values. The CFD-result averaged *Po* value was 4.19 for the RuT and 5.22 for the DDT impeller. These values were lower than the experimental one by approximately18% for the RuT and 14% for the DDT impeller. The differences, which are consistent for a given *Re* range, can be attributed to the turbulence model that was used (under-prediction of the turbulence intensity by the k–ε mode[18]), as well as the wall functions (the velocity gradients used in the calculation of the shear force are estimated according to the hybrid wall-functions approach[22]), the chosen grid density near the impeller and the vessel wall (the first cell is in the range of wall-function applicability) used, and the chosen model of impeller rotation (MRF) as well as other details.[26] Better agreement can be found in work of Taghavi et al.[28], where the CFD-calculated Power number was only smaller by 1.6–4.5% than the measured value, and so good results were obtained with LES modeling.

3. 2. Mixing Time

The experimental mixing-time dependence vs. power dissipation is shown in Figure 7. If we consider that all the mixing times were determined using the same experimental technique and set-up, some trends can be seen clearly: (i) in general, the higher the dissipated power, the smaller the mixing time, and, (ii) shorter times at the same power dissipation were achieved with the DDT impeller, especially for lower power dissipation. The reason can be found in fact that the DDT impeller, due to its construction, achieved a higher pumping capacity and less turbulence than the RuT impeller. As was clear from visual ob-

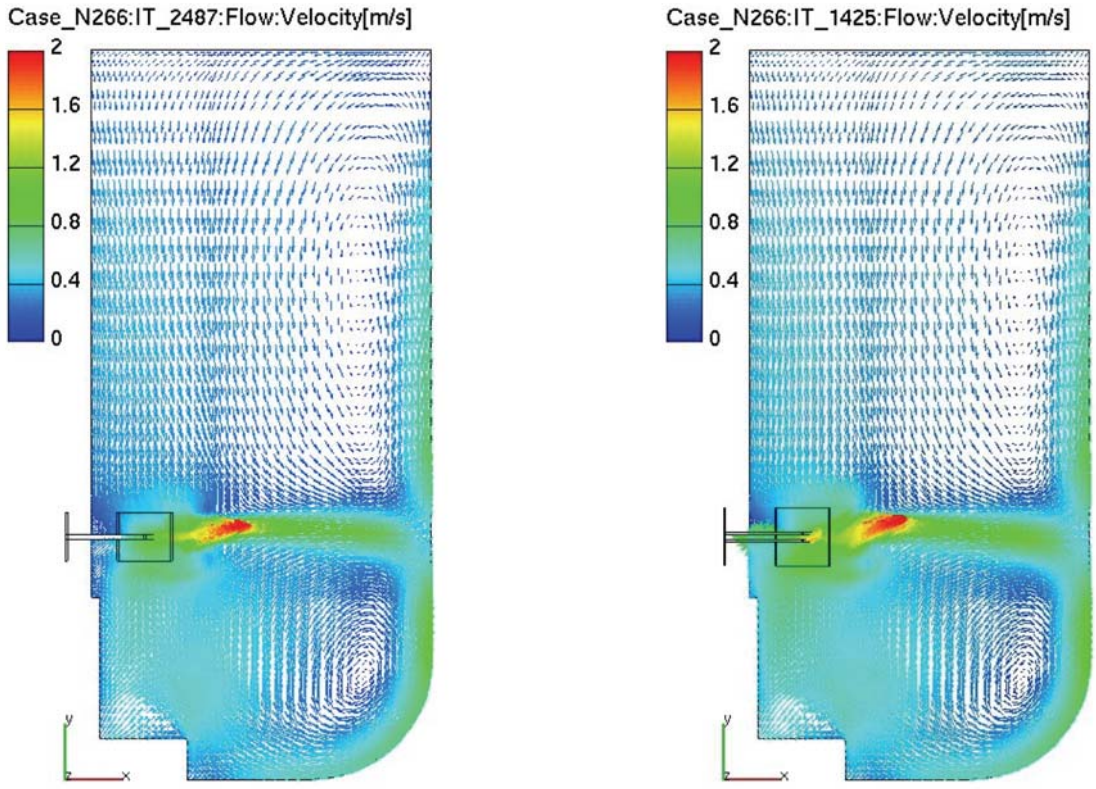

Figure 6. Velocity field of the RuT (left) and the DDT (right) impellers for n = 266 min^{-1}

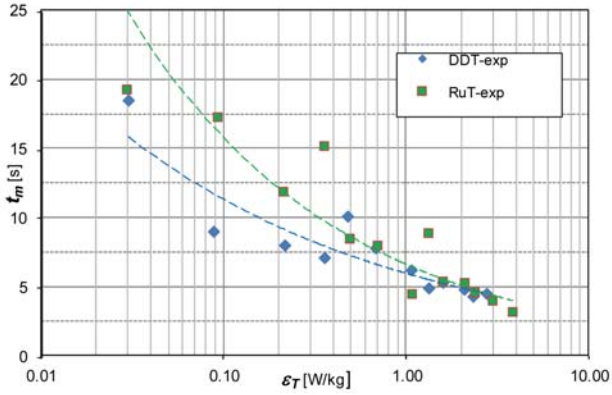

Figure 7. Comparison of experimental mixing times – (curves fitted by Eq.12)

servations through the vessel wall, as well as with CFD results, both impellers produced a strong radial discharge flow, reaching the vessel wall divided into an upper and lower circulation loop. The DDT impeller causes, due to its double-disk construction and higher blades, a much wider area of discharge flow than the RuT impeller at same impeller speed, which is reflected in a higher *Po* number. Taking into account that pumping capacity is the main contribution to the mixing time (macro-mixing), shorter mixing times are justified for the DDT impeller. There have been similar findings[14] where different single impellers achieved various mixing times for equal power dissipation as well as in mixing with various dual impellers.[5]

CFD approach For a given set of impeller speeds various CFD-predicted mixing times (temperature responses) at the thermocouple location are indicated in Figure 8. It is clear that shorter times were achieved at higher impeller speeds.

The CFD approach enabled a qualitative and quantitative insight into the progress of mixing for the added water in the time-space domain and for the experiment can be, according to the 'what you see' criterion, very similar to the de/colorization technique. In our case, the mixing progress of added hot water in a given location for an impeller speed of 266 min^{-1} can be seen in Figure 9 for the RuT impeller and in Figure 10 for the DDT one. Here, the red color represents a temperature fluctuation higher than +5% and the blue one, higher than –5%. The turbulent mixing process consists of two basic mechanisms for the added water transport: convection (by mean flow) and turbulent (eddy) diffusion. As can be seen in Figures 9 and 10, the added water is transported in the tangential direction below the liquid surface and also in the axial direction towards the impeller. In this region of the tank, convective transport plays an important role because the levels of turbulence are low compared with those in the impeller region, as revealed by the flow calculation (Figure 6). When the added water reaches the impeller, it is transported towards the tank wall by the impeller discharge flow and divided upwards and downwards along the wall. Due to the high levels of turbulence in the impeller discharge flow and in the flow along the tank wall dispersion of added water (tracer in general) the (eddy) turbulent diffusion plays an important role. With time, the added water is conveyed towards the liquid free surface as well as towards the bottom of the tank by the recirculation loop in the upper and lower parts of the tank. In this particular case the local mixing time is achieved in about 11.7 s. The predicted evolution of the local mixing progress in the tank qualitatively resembles studies in equal or similar mixing arrangements.[18,19,23]

From the further development of the mixing it follows that the homogeneity level due to mixing is achieved in the lower part of vessel first, and then later in the upper part. For the observed case, the corresponding mixing time satisfied the condition of Eq.5 at a given location, while mixing in close surroundings is still in progress, as depicted in Figures 9 (t_m = 12 sec) and 10 (t_m = 11 sec). This finding led to the conclusion that the local mixing time can only be taken as a rough measure of mixing quantification.

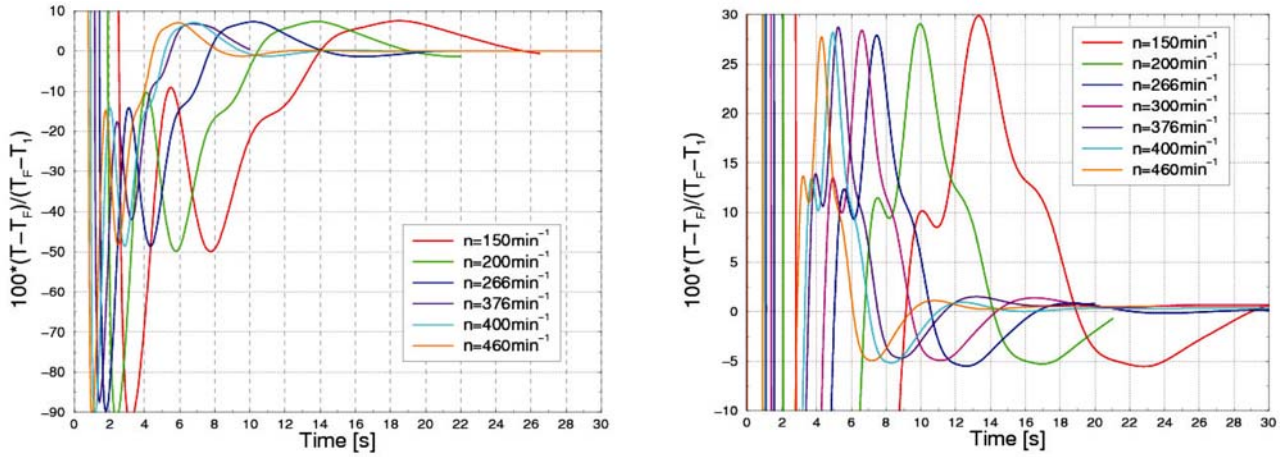

Figure 8. Mixing time for various impeller speeds: RuT (left) and DDT (right)

As already shown, the RuT and DDT impellers achieved different mixing times for the same power dissipation. In general, the experimental mixing times and the CFD-calculated ones were in fair agreement. The latter were probably due to the 'frozen' velocity field technique (which enabled a many-times-shortened computational time) consistently higher than the experimental ones, i.e., on average by 24% for the RuT impeller and 46% for the DDT impeller. The reason can be also found in the insufficiency of the k–ε turbulence model (which may not always capture the effects of strong streamline curvature and impingement), as well as the use of the wall functions (instead of integration up to the wall, which may improve the results, especially in the narrow gap between the disks of DDT), the grid density

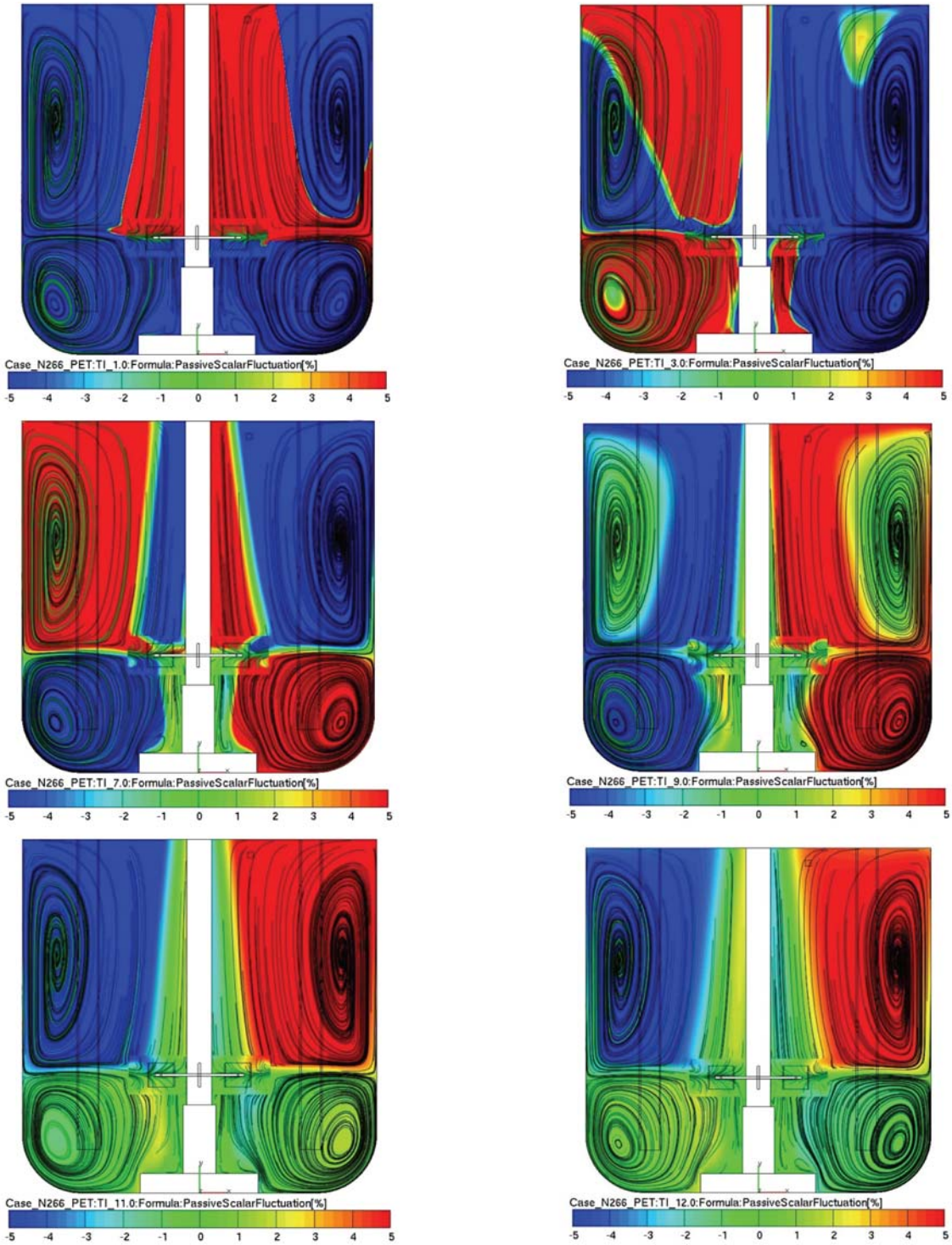

Figure 9. Predicted mixing process as a function of time in the 0–180° vertical plane for the RuT impeller

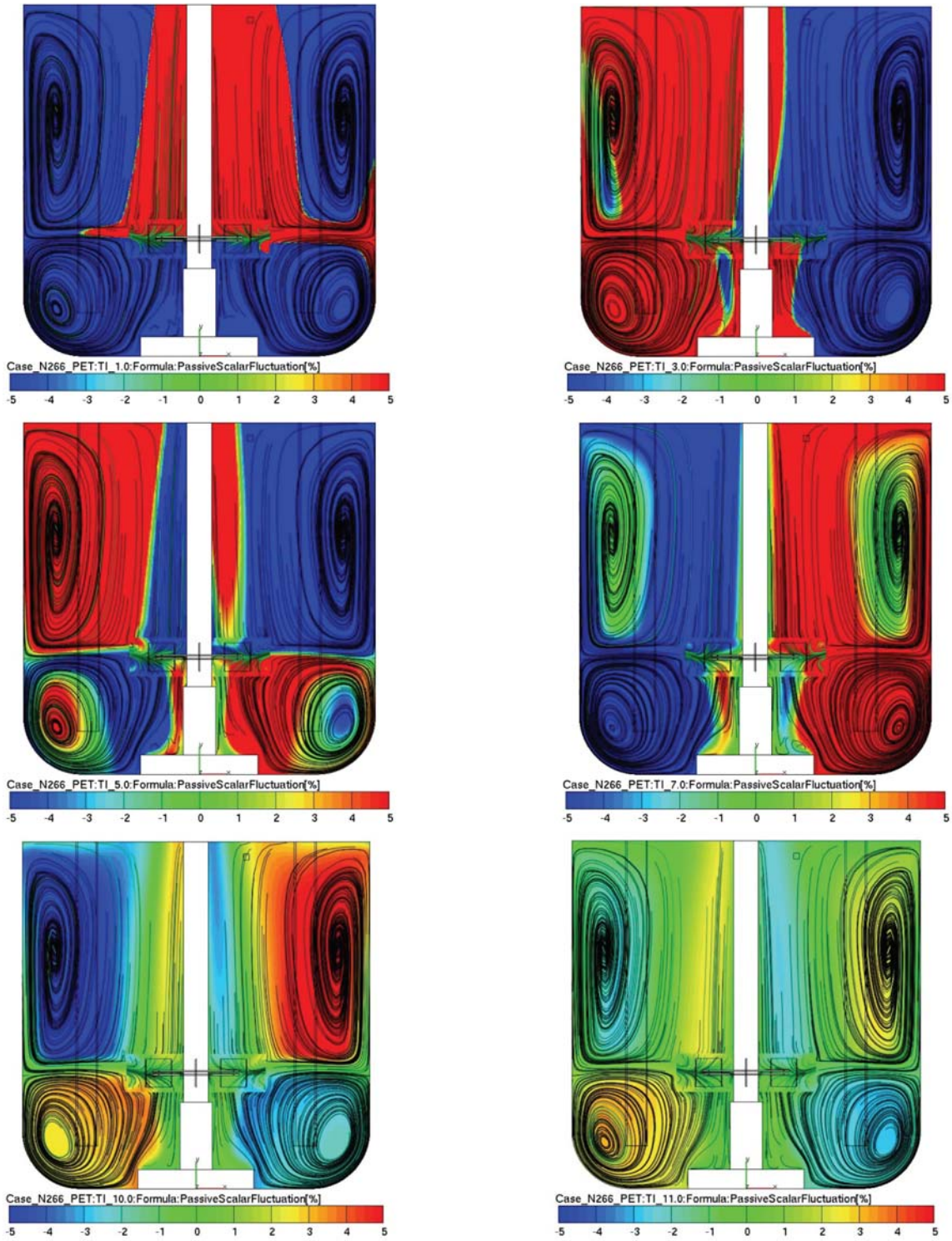

Figure 10. Predicted mixing process as a function of time in the 0–180° vertical plane for the DDT impeller

near the shaft and the vessel wall (which is difficult to adjust so as to keep y+ in a narrow range over all the studied operating regimes), etc. There were similar findings,[18] where the CFD-determined mixing times using the k–ε turbulence model were also higher than the experimental ones. According to the literature[14,18,23,27] the mixing time measured at different locations can vary in the range between 11% and 40%. In liquid mixing with multiple impellers[24] the CFD-analyzed mixing times were as much as 2-3 times longer than the experimental ones.

Table 1. Comparison of experimental and CFD-analyzed mixing times

Impeller speed	Experimental mixing time (s)		CFD-analyzed mixing time (s)		Relative difference $(t_{ex} - t_{CFD})/ t_{ex}$	Relative difference $(t_{ex} - t_{CFD})/ t_{ex}$
n (min^{-1})	**RuT**	**DDT**	**RuT**	**DDT**	**RuT**	**DDT**
150	17.3	9.0	21.2	18.1	–0.225	–1.011
200	11.9	8.0	15.8	13.5	–0.327	–0.687
266	8.5	10.0	11.7	10.0	–0.376	0
376	8.9	4.9	8.1	7.2	0.089	–0.469
400	5.4	5.3	7.8	6.6	–0.444	–0.245
460	4.6	4.3	6.8	5.8	–0.147	–0.349

The CFD-predicted mixing times are presented together with the experimental ones in Table 1. Shorter times were achieved with the DDT impeller, i.e., an average of 14% compared to the RuT impeller. A similar situation was found for the experimental data. Regardless of whether the measurements were performed only at one location, it is again clear that the type of impeller did influence the mixing time for the same power dissipation. This is in good agreement with the literature results, where mixing time was found to be closely related to the impeller's design.[5,14,26]

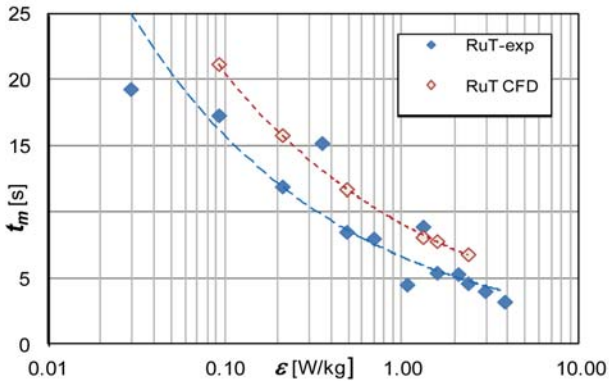

Figure 11. Experimental and CFD predicted mixing time for the RuT impeller – (curves fitted by Eq.12)

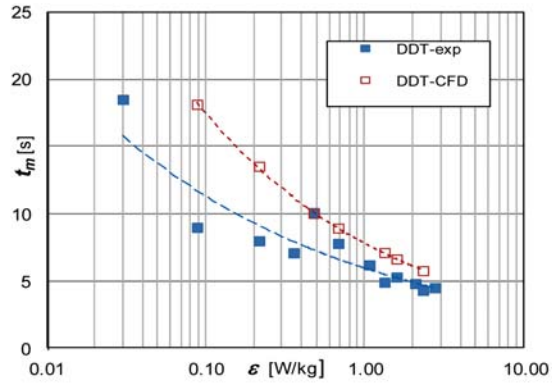

Figure 12. Experimental and CFD-predicted mixing time for DDT impeller – (curves fitted by Eq.12)

As can be seen from Figures 11 and 12 the CFD-predicted times are longer than the measured ones, i.e., for the RuT impeller, by an average of 24%, and for the DDT impeller, by an average of 46%. The results show reasonable agreement; however, the over prediction of the mixing time can be attributed to the under-prediction of the turbulence intensity by the k–ε model, which is based on the Reynolds-averaged Navier–Stokes equations.[18]

To compare our results with those found in the literature seems to be an impossible task. This is because the techniques, measuring locations, mixing-degree criterion as well as the mixing equipment with various scales and geometrical ratios differ from article to article. Narrowing to the turbulent regime the recommendation[30] was given based on a variety of impeller types with various diameters/vessel ratios and impeller positioning. To reach 95% homogeneity for all the impellers at all scales and $H=T$ the following criterion for the mixing time is available:

$$t_m = A \cdot T^{2/3} \cdot \varepsilon^{-1/3} \cdot \left(D/T\right)^{-1/3} \tag{11}$$

for the condition $1/3 \leq D/T \leq 1/2$. Equation 11 implies that all impeller types of equal impeller-to-tank diameter ratio are equally energy efficient in achieving an overall homogenization and actually enable an estimation of the global mixing time representing the whole vessel. Rearranging Eq.11 with the original constant A = 5.9 gives for D/T = 0.33 and T = 0.45 m and our geometrical parameters the following form:

$$t_m = a\ \varepsilon^b, \tag{12}$$

with a = 4.997 and b = –0.333. The values of the experimental and CFD-obtained local mixing times were correlated using Eq.12 based on the root-mean-square method. The correlation factor R and the coefficients are given in Table 2. It is clear that the mixing time varies with a power of between –0.279 and –0.379 of the mixing power dissipation (per unit mass of the liquid) for the experimental results and is approximately –0.35 for the CFD analy-

sis. The constants in the proportionality relationship are found to be impeller-design dependent.

Table 2. Parameters of correlation Eq. (12)

Impeller	*a*	*b*	*R*
RuT-exp	6.607	– 0.378	0.923
DDT-exp	5.949	–0.279	0.926
RuT-CFD	9.110	– 0.353	0.999
DDT-CFD	7.804	–0.350	0.999

In Figure 13 the correlation of the CFD-analyzed mixing times vs. the specific power is presented. Smaller mixing times are evident for the DDT impeller, especially for a lower specific power. The findings are similar to the experimental results and the literature data, where various studies reported the effect of impeller design on the mixing time and the power consumption.[5,9,14,31] On the other hand, some studies led to the same mixing time, irrespective of the impeller design for the same power consumption.[4,6,30] Recently, a critical analysis[26] has been presented which shows that the liquid-phase mixing in the turbulent flow regime is a flow-controlled process and hence depends on the impeller design.[13,18] It was found that the mixing time varies inversely with the cube root of the power consumption per unit volume of the liquid. The constants in the proportionality relationship are found to be impeller-design dependent.

Fassano and Penney,[31] based on an idealized mixing decay model, developed a correlation to calculate the time required to reach a certain degree of homogeneity of the mixture in the agitated vessel:

$$t_m = \frac{-\ln(1-u)}{K \cdot n \cdot (D/T)^p \cdot (T/H)^{0.5}} \quad (13)$$

where K and p denote the impeller-type constants (1.06 and 2.17 for the RuT impeller) and u the degree of uniformity of the mixture (in our case 0.95) in a stirred vessel.

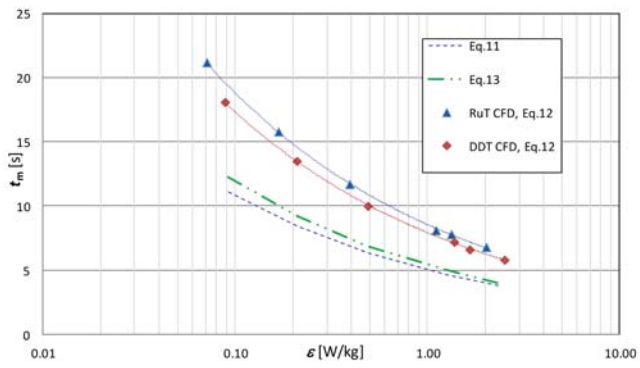

Figure 13. Comparison of the correlated results of the mixing time

The resulting mixing times for the RuT impeller are given in Figure 13 as a comparison with our correlated results.

Our results for the RuT impeller can be compared with those found in the literature[38] for similar hydrodynamic regimes. Here, the measured and the CFD-predicted *Po* values were found to be 5.0 and 4.85, and were close to our values of 5.15 and 4.19, respectively. In both cases the under prediction of the turbulence intensity caused lower Po numbers. In the same study[38] the mixing-time data were obtained using conductivity metering (CM), the decolourization method (DM) and the CFD prediction. With the CM method the tracer was detected at a point located near the surface and close to the wall between the two baffles. Table 4 shows that the mixing times based on the conductivity and decolourization methods were similar and are close to our experimental values, which are also in agreement with the literate data.[5,37] The experimental mixing times were shorter than the times obtained using the CFD simulation, but were longer than those obtained using the empirical models. Of the two models, the Nienow model gave a shorter mixing time than that of the Fasano and Penney model.[31] The trends were qualitatively similar for all three configurations, as shown in Table 3.

The measuring location should have the same relative position (r/T, z/T, φ) to enable a comparison of the results with the literature data.[14,18,23] In accordance with the recommendations for the design of the agitators for blending,[14,30] three different measuring locations were prescribed: (i) $T/4.5$ below the liquid surface and $T/4.7$ from the shaft axis, (ii) $T/50$ below the impeller and $T/8$ from the shaft axis, and (iii) behind a baffle at $T/2.2$ from the shaft axis and T/3 below the liquid surface. Haucine et al.[14] reported the mixing times at particular locations where the mixing times vary between 3.7% in case (i), –10.1% in case (ii) and 6.5% in case(iii), compared to the average of all three locations. We had similar findings for our comparison of the CFD-analyzed mixing times for the RuT impeller: 4.4% in case (i), –16% in case (ii) and +11.3% in case (iii).

On the other hand, the probe locations are, in most cases, set individually, such as 32 locations in Diestelhoff et al.,[35] provided with all the geometrical details and a description of the injection points. To compare our CFD mixing-time results for the RuT impeller with those found in the literature, the experimental data of Diestelhoff et al.[35] and the CFD-calculated data of Javed et al.[20] were taken. A comparison with our results is possible at only one impeller speed, i.e., $n = 266$ min^{-1}, which corresponds to a Reynolds number of 99134 and is similar to $Re_{Jav} = Re_{Die} = 96393$. A dimensionless time $n \cdot t_m$ is shown in Table 4 for the original set of positions in the r-z plane by $\varphi = 0°$ and 180°.

Very good agreement can be found by comparing the by-position averaged $n \cdot t$ of Javed et al. and our data, which were 26.9 and 26.8, respectively. As can be seen

Table 3. Experimental and simulation mixing times for the RuT impeller

Method	*Re*	*T* (m)	$n \times t_m$	No. of measuring points, position
Kraume et al.[37] DM & CM exp.	$2 \cdot 10^4 – 2{,}6 \cdot 10^5$	0.40	35	DM, *"visually observed throughout the whole vessel…"*
				CM /
Present work – exp.	74257	0.45	39.7	1 point, (*r*,*z*; 65,420 mm), between two baffles
Ochieng & Onyango[38] – CM exp	79000	0.38	33.0	1 point, "*near the surface, close to the wall, between two baffles*"
Ochieng & Onyango[38] – DM exp	79000	0.38	32.0	1 point, "*near the surface, close to the wall, between two baffles*"
Ochieng & Onyango[38] – CFD	79000	0.38	65.6	1 point, "*near the surface, close to the wall, between two baffles*"
Present work – CFD	74257	0.45	52.7	1 point, (*r*,*z*; 65,420 mm), between two baffles
Ochieng et al.[18] – CFD	66900	0.38	50	1 point, "*near the surface, close to the wall, between two baffles*"
Fassano & Penney model[31]	74257	0.45	30.7	/
Nienow model	74275	0.45	28.0	/

Table 4. Dimensionless mixing times for the RuT impeller

Meas. position	*r/T*	*z/H*	Javed et al[20]. et al. $n \times t_{mod}$	Diestelhoff et al.[20] $n \times t_{exp}$	our CFD $n \times t_{mod}$
A	0.126	0.667	31.0	31.0	26.0
B	0.252	0.667	28.0	33.5	31.7
C	0.360	0.667	22.0	30.0	34.4
D	0.469	0.667	29.0	29.0	31.3
G	0.126	0.190	29.0	30.5	18.7
H	0.252	0.190	27.0	26.5	23.1
I	0.360	0.190	25.0	33.5	25.3
J	0.469	0.190	24.0	25.5	23.7

from Figure 14, the largest variation was at point C, in the area where the last homogenization process took place, as can be seen see in Figure 9.

In some other studies[6,7,38] the measuring locations are mentioned only in an informative manner or even without any location information given at all,[19] which means that any comparison with these data is impossible.

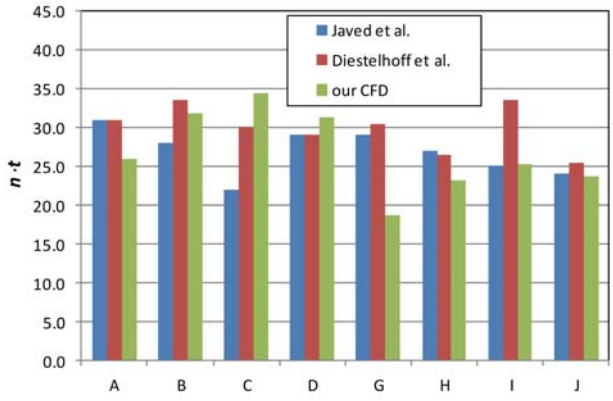

Figure 14. Experimental and CFD-analyzed dimensionless mixing time

4. Conclusions

The objectives of this work were to study the dissipated power and local mixing time of a standard Rushton turbine and a modified double-disk impeller when stirring in water. The results were obtained from: (a) measurements on the experimental set-up and (ii) a CFD analysis. The power dissipation was based on rotational-torque and impeller-speed measurements, while the mixing time was measured using the pulse-response technique. In order to calculate the mixing power and the mixing time in a stirred vessel the commercial AVL CFD code was used. The multiple reference frame technique was employed. The mixing power was evaluated on the basis of the torque exerted on the impeller and shaft surfaces. The mixing time was estimated using the same principle as for the measurements, applied in the same location. The selected "frozen-flow" field-calculation procedure resulted in a considerable reduction in the required CPU time. The error introduced due to the treatment of temperature (as a passive scalar) was, for the purpose of design comparisons, found to be acceptable.

The power-number values given by the CFD calculation were consistently lower than the measured ones, i.e., ~18% for the RuT and ~14% for the DDT. The reason

can be found in the turbulence model (Standard k–ε) and the hybrid wall-function approach, chosen due to its robustness and moderate CPU demand. The calculated local mixing times are in fair agreement with the measured values, thus confirming the applicability of the chosen methodology. The results are consistently higher by approximately 24% for the RuT impeller and 46% for the DDT impeller. These fluctuations could be attributed to the already-mentioned "frozen-flow" field strategy, the chosen turbulence model, the wall-functions approach, the achievable mesh density – especially near the wall, etc. As expected, the mixing times become shorter as the impeller's rotational speed increases.

5. Acknowledgments

This work was financially supported by the Slovenian Ministry of Higher Education, Science and Technology under contract No. P2-0162.

Notation

D = impeller diameter, m
g = gravity, m/s^2
H = liquid height, m
l = blade length, m
m_L = mass of liquid, kg
M = measured torque, Nm
n = rotational impeller speed, s^{-1}
P = mixing power, W
T = tank diameter, m; temperature, K
t_m = mixing time, s
w = blade width, m
$C_{\varepsilon i}$ = model constants
V_i = relative velocity,
p = pressure, Pa
x_i = positional vector, m
U_i = velocity vector, m/s
k = turbulence kinetic energy, m^2/s^2
$\boldsymbol{r}$ = distance vector, m
$\boldsymbol{F}$ = shear force, N
S_{ij} = mean rate of strain tensor, 1/s
Fr = Froude no., $n^2 \cdot D/g$
Re = Reynolds no., $n \cdot D^2/\nu$
Po = Power no., $P/(\rho \cdot n^3 \cdot D^5)$
ε = power dissipation per mass of liquid, W/kg
ρ = liquid density, m^3/kg
ν = kinematic viscosity, m^2/s
μ = dynamic viscosity, Pas
ω_i = vorticity, 1/s
ε_{ijk} = permutation symbol
λ = heat conductivity, W/mK
μ_t = turbulent viscosity, Pas
σ_k = turbulent Prandtl number, –
τ = calculated torque, Nm

6. References

1. Bujalski, J. M., Jaworski, Z., Bujalski, W., Nienow, A. W., *Chem. Eng. Res. Des.,* **2002,** *80,* 824–831.
2. Bombač, A., Žun, I., *J. Mech. Engng.*, **2002**, *48,* 663–676.
3. Bombač, A., *J. Mech. Engng.,* **1998**, *44,* 105–116.
4. Nienow, A. W., *Chem. Eng. Sci.,* **1997,** *52,* 2557–2565.
5. Bouaifi, M., Roustan, M., *Chem. Eng. Process.,* **2001**, *40,* 87–95.
6. Vasconcelos, M. T. J., Orvalho, S. C. P., Rodrigues, M. A. F., Alves, S. S., *Ind. Eng. Chem. Res.*, **2000**, *39,* 203–213.
7. Guillard, F., Trägårdh, C., *Chem. Eng. Process, Process Intensification*, **2003**, *42,* 373–386.
8. Moucha, T., Linek, V., Prokopova, E., *Chem. Engng. Sci.*, **2003**, *53,* 603–615.
9. Pinelli, D., Bakker, A., Myers, K. J., Reeder, M. F., Fasano, J., Magelli, F., *Trans. lChemE.*, **2003**, *81-A,* 448–454.
10. Bombač, A., Žun, I., in Magelli, F., Baldi, G., Brucato, A. (Eds.), *Proceedings of the 12th European Conference on Mixing, Bologna, Italy, 27–30 June*, **2006**.
11. Chen, Z. D., Chen, J. J. J., *Trans. IChemE.*, **1999**, *77,* 104–109.
12. Roman, R.V., Tudose, R. Z., *Chem. Engng J.*, **1996**, *61,* 83–93.
13. Jing ZHAO, Zhengming GAO, Yuyun BAO, *Chinese J. Chem. Engng.*, **2011**, *19,* 232–242.
14. Haucine, I., Plasari, E., David, R., *Chem. Eng. Technol.*, **2001**, *23,* 605–613.
15. Karcz, J, Major, M., *Chem. Engng. Proc.*, **1998**, *37,* 249–256.
16. Wei-Ming Lu, Hong-Zhang, Ming-Ying Ju, *Chem. Engng. Sci.,* **1997,** *52,* 3843–3851.
17. Ando, K., Obata, E., Ikeda, K., Fukuda, T., *Can. J. Chem. Engng.*, **1990**, *68,* 278–283.
18. Ochieng, A., Onyango, M. S., Kumar, A., Kiriamiti, K., Musonge, P., *Chem. Engng. Proc.*, **2008**, *47,* 842–851.
19. Zhang, Q., Yong, Y., Mao, Z. S., Yang, C., Zhao, C., *Chem. Engng. Sci.*, **2009**, *64,* 2926–2933.
20. Javed, K. H., Mahmud, T., Zhu, J. M., *Chem. Engng. Proc.*, **2006**, *45,* 99–112.
21. Levenspiel, O., *Chemical Reaction Engineering.* 3rd Ed., Wiley & Sons, New York, **1999**.
22. AVL Fire, Manual pages, AVL LIST GmbH, **2009**.
23. Yeoh, S. L., Papadakis, G., Yianneskis, M., *Chem. Eng. Sci.*, **2005**, *60,* 2293–2302.
24. Jaworski, Z., Bujalski, W., Otomo, N., Nienow, A. W., *Trans. IChemE.*, **2000**, *78,* 327–333.
25. Chen, Z. D., Chen, J. J. J., *Trans. IChemE.*, **1999**, *77,* 104–109.
26. Joshi, J. B., Nere, N. K., Rane, C. V., Murthy, B. N., Mathpati, C. S., Patwardhan, A.W., Ranade, V. V., *Can. J. Chem. Engng.*, **2011**, *89,* 23–82.
27. Montante, G., Moštek, M., Jahoda, M., Magelli, F., *Chem. Eng. Sci.*, **2005**, *60,* 2427–2437.
28. Taghavi, M., Zadghaffari, R., Moghaddas, J., Moghaddas, Y., *Chem. Engng. Res. Des.*, **2011**, *89,* 280–290.

29. Bombač, A., Žun, I., Filipič, B., Žumer, M., *AIChE J.*, **1997**, *43,* 2921–2931.
30. Grenville, K. R., Nienow, A. W., in Paul, E. L., Atiemo-Obeng, V. A., Kresta, S. M. (Eds.) Wiley-Interscience, Hoboken, **2004**, pp.507–542.
31. Fasano, J.B., Penney, W. R., *Chem. Engng. Prog.*, **1991**, *57,* 56–63.
32. Basara, B., Alajbegovic, A., Beader, D., *Int. J. Numer. Meth. Fluids*, **2004**, *45,* 1137–1159.
33. Bombač, A., Beader, D., Žun, I., *Ventil*, **2009**, 15, 526–535.
34. Slemenik, L., Žumer, M. *Acta Chim. Slov.*, **2001**, *48,* 265–278.
35. Distelhoff M. F. W., Marquis, A. J., Nouri, J. M., Whitelaw, J. H., *Can. J. Chem. Eng*., **1997**, *75,* 641–652.
36. Bombač, Andrej, Žun, Iztok. Individual impeller flooding in aerated vessel stirred by multiple-Rushton. *Chem. Eng. J.*, **2006**, *116,* 85–95.
37. Kraume, M., Zehner, P., *Chem. Eng. Res. Des.*, **2001**, *79,* 811–818.
38. Ochieng, A., Onyango, M. S., *Chem. Engng. and Proc.*, **2008**, *47,* 1853–1860.
39. Alves, S. S., Vasconcelos, J. M. T., Barata, J., *Chem. Eng. Res. Des*., **1997**, *75,* 334–338.
40. Zadghaffari, R., Moghaddas, J. S., Revstedt J., *Comput. & Chem. Engng.*, **2009**, *33,* 1240–1246.
41. Joshi, J. B., Ranade, V. V., *Ind. Eng. Chem. Res.* **2003**, *42,* 1115–1128

Povzetek

Predstavljena je analiza časov pomešanja pri mešanju kapljevine v posodi s turbinskim mešalom z dvema diskoma (DDT, SI Pat.No. 22243) in s splošno znanim Rushtonovim mešalom (RuT). Čas pomešanja je bil merjen lokalno na osnovi metode motnja/odziv. Manjša količina vroče vode, vlita v kapljevino tik nad merilno lokacijo, predstavlja vneseno motnjo, medtem ko sprememba temperature kapljevine predstavlja odziv sistema. Rezultati časov pomešanja so bili dobljeni na dva načina: (i) iz meritev na preizkusni napravi in (ii) izračunani s programskim paketom računalniške dinamike tekočin (CFD). Pri CFD izračunu je bilo vlitje vroče vode v kapljevino numerično simulirano z inicializacijo skalarnega polja. Čas inicializacije temperaturne motnje je v območju dolivanja ustrezal času vlitja pri eksperimentu. Pri tem je celotno dovedeno toploto nemoteno odnašal tok. Rezultati časov pomešanja dobljeni s CFD so sistematično daljši od izmerjenih na preizkusni napravi pri vseh režimih mešanja, od 150 do 450 vrt/min. Iz primerjave naših rezultatov časov pomešanja z vrednostmi po literature ugotovimo dokaj dobro ujemanje.